The wasting-associated metabolite succinate disrupts myogenesis and impairs skeletal muscle regeneration

Paige C Arneson[1], Kelly A Hogan[1], Alexandra M Shin[1], Adrienne Samani[1], Aminah Jatoi[2], Jason D Doles[1]*

[1]Department of Biochemistry and Molecular Biology, Mayo Clinic, Rochester, Minnesota, 55905 USA. [2]Department of Oncology, Mayo Clinic, Rochester, Minnesota.

*Corresponding Author:
Jason D Doles
Department of Biochemistry and Molecular Biology
Mayo Clinic
200 First St SW
Guggenheim 16-11A1
Rochester, MN 55905
Tel: (507) 284-9372
Fax: (507) 284-3383
E-mail: Doles.Jason@mayo.edu

ABSTRACT

Background: Muscle wasting is a debilitating co-morbidity affecting most advanced cancer patients. Alongside enhanced muscle catabolism, defects in muscle repair/regeneration contribute to cancer-associated wasting. Among the factors implicated in suppression of muscle regeneration are cytokines that interfere with myogenic signal transduction pathways. Less understood is how other cancer/wasting-associated cues, such as metabolites, contribute to muscle dysfunction. This study investigates how the metabolite succinate affects myogenesis and muscle regeneration.

Methods: We leveraged an established ectopic metabolite treatment (cell permeable dimethyl-succinate) strategy to evaluate the ability of intracellular succinate elevation to 1) affect myoblast homeostasis (proliferation, apoptosis), 2) disrupt protein dynamics and induce wasting-associated atrophy, and 3) modulate *in vitro* myogenesis. *In vivo* succinate supplementation experiments (2% succinate, 1% sucrose vehicle) were used to corroborate and extend *in vitro* observations. Metabolic profiling and functional metabolic studies were then performed to investigate the impact of succinate elevation on mitochondria function.

Results: We found that *in vitro* succinate supplementation elevated intracellular succinate about 2-fold, and did not have an impact on proliferation or apoptosis of C2C12 myoblasts. Elevated succinate had minor effects on protein homeostasis (~25% decrease in protein synthesis assessed by OPP staining), and no significant effect on myotube atrophy. Succinate elevation interfered with *in vitro* myoblast differentiation, characterized by significant decreases in late markers of myogenesis and fewer nuclei per myosin heavy chain positive structure (assessed by immunofluorescence staining). While mice orally administered succinate did not exhibit changes in overall body composition or whole muscle weights, these mice displayed smaller muscle myofiber diameters (~6% decrease in the mean of non-linear regression curves fit to the histograms of minimum feret diameter distribution), which was exacerbated when muscle

regeneration was induced with barium chloride injury. Significant decreases in the mean of non-linear regression curves fit to the histograms of minimum feret diameter distributions were observed 7 days and 28 days post injury. Elevated numbers of myogenin positive cells (3-fold increase) supportive of the differentiation defects observed *in vitro* were observed 28 days post injury. Metabolic profiling and functional metabolic assessment of myoblasts revealed that succinate elevation caused both widespread metabolic changes and significantly lowered maximal cellular respiration (~35% decrease).

Conclusions: This study broadens the repertoire of wasting-associated factors that can directly modulate muscle progenitor cell function and strengthens the hypothesis that metabolic derangements are significant contributors to impaired muscle regeneration, an important aspect of cancer-associated muscle wasting.

Keywords: Muscle wasting, skeletal muscle, succinate, myogenesis

INTRODUCTION

Lean mass (muscle) loss and functional skeletal muscle decline affect the majority of advanced cancer patients and are associated with poor prognosis and quality of life. Reversing muscle loss in tumor-bearing animal models leads to improved chemotherapeutic efficacy, reduced cancer-associated morbidity, and prolonged survival[1,2], demonstrating that maintaining muscle mass in cancer patients should be a top clinical priority. Despite a growing number of active clinical trials for cancer-associated weight loss, effective therapies remain elusive. Major problems hampering significant progress include the variability of weight loss presentation across tumor types and stages, limited early detection of lean mass/adipose tissue loss, and a poor understanding of the molecular underpinnings of this complex syndrome. More work is needed to identify and target alterations in skeletal muscle that contribute to overall tissue decline in cancer patients.

Multiple factors produced by both tumor and host contribute to the wasting state. Many identified 'wasting factors' are cytokines/chemokines such as TNF-alpha, Interleukins (including IL-1 and IL-6), CXC-proteins, and TGF-β[3-6], and are known to accelerate muscle atrophy, promote protein breakdown, and inhibit muscle regeneration. Additionally, many of these factors are linked to mitochondria dysfunction and altered cellular metabolism[7]. Indeed, metabolic regulation of skeletal muscle function has come into focus as a major driver of multiple aspects of muscle biology including catabolism, hypertrophy, and regenerative capacity. Examples of metabolic processes linked to cancer-associated muscle wasting are: mitochondria dynamics[8], mitochondria biogenesis[9,10], mitochondria catabolism (ie. mitophagy)[11], and compromised energy utilization pathways[12]. A more sophisticated understanding of how metabolic factors contribute to cancer-associated muscle dysfunction is needed to facilitate the development of novel therapies to preserve muscle mass and function in cancer patients.

73 Succinate is a metabolite best known for its role as a TCA cycle intermediate
74 and central player in mitochondria metabolism and ATP generation. Recently,
75 new roles for succinate have emerged and include immune cell modulation[13],
76 HIF-1a stabilization in cancer[14], epigenome remodeling via inhibition of alpha-
77 ketoglutarate dependent dioxygenases[15], and post-translational protein
78 modification (succinylation)[16]. This expanding repertoire of cellular activities
79 suggests a broader role for succinate in regulating cellular processes such as
80 differentiation, fate decisions, and survival. Interestingly, a recent study reported
81 serum succinate accumulation as a biomarker capable of distinguishing non-
82 wasting, tumor-bearing, and tumor-bearing with weight loss patients[17]. In the
83 present study, we sought to determine if succinate elevation directly impacts
84 muscle cell function, with a particular emphasis on myogenic differentiation given
85 prior studies linking succinate levels to cell fate decisions[18,19].

86 Alterations in the balance between muscle breakdown and
87 repair/regeneration underlie cancer-associated muscle wasting. While catabolic
88 pathways have historically received the most attention in the muscle wasting
89 field, processes leading to the suppression of muscle regeneration are
90 understudied despite their clear contribution to the etiology of muscle wasting[20].
91 Central to the process of muscle regeneration is the skeletal muscle stem cell, or
92 satellite cell. In healthy muscle, satellite cells contribute to tissue maintenance
93 and actively participate in muscle homeostasis[21,22]. When challenged by injury
94 stimuli, satellite cells activate, proliferate, and differentiate into mature muscle
95 cells in order to facilitate muscle repair and regeneration. Indeed, genetic
96 ablation experiments show that Pax7+ stem/satellite cells are required for muscle
97 regeneration following major trauma[23-25]. Defects in satellite cell function and/or
98 regeneration are associated with a growing list of muscle atrophy states including
99 disuse[26,27], denervation[28,29], chronic obstructive pulmonary disease (COPD) [30],
100 burn injury[31,32], diabetes[33,34], chronic kidney disease[35], and hepatic disorders[36],
101 although the precise role of impaired repair/regeneration in each of these disease
102 states remains unclear. In cancer, multiple studies show that muscle
103 regeneration is linked to functional skeletal muscle deficits and propose that

104 mononuclear muscle progenitor cells drive aspects of the atrophy phenotype[37,38].
105 Taking into account the expanding role of the satellite cell in muscle wasting, the
106 importance of metabolism in cancer-associated wasting, and recent evidence
107 implicating the metabolite succinate in cancer cachexia[17] and stem/progenitor
108 cell function[18,19], we sought to characterize the effects of succinate elevation on
109 muscle myoblast cell dynamics (*in vitro*) and muscle homeostasis (*in vivo*).
110 Studies presented herein highlight the ability of a metabolite – succinate – to
111 directly impact myogenesis and muscle regeneration. This underscores the need
112 to further explore metabolic drivers of impaired muscle regeneration and muscle
113 catabolism, both contributors to cancer-associated muscle wasting, in order to
114 advance anti-wasting cancer therapies.

115 **METHODS**

116 **Animals**

117 Mice were bred and housed according to NIH guidelines for the ethical treatment
118 of animals in a pathogen-free facility at the Mayo Clinic (Rochester, MN campus).
119 The Mayo Clinic Institutional Animal Care and Use Committee (IACUC) approved
120 all animal protocols and all experiments were performed in accordance with
121 relevant guidelines and regulations. Wild type mice were on the FVB background
122 (Charles River Labs) unless noted otherwise in the text or figure legends. For
123 homeostasis and regeneration assays, all mice were 3-5 months old, FVB males.
124 In these experiments, mice were administered succinate (Sigma-Aldrich) (2%)
125 and 1% sucrose (vehicle) or 1% sucrose (vehicle only) in their drinking water for
126 6-8 weeks prior to and throughout the injury time course. Muscle injury was
127 performed by injecting the left *tibialis anterior* muscle with 70uL $BaCl_2$ (1.2% in
128 saline) or saline (control) and harvesting muscles 1 or 4 weeks post injury.

129 **EchoMRI imaging**

130 An EchoMRI (magnetic resonance imaging) Body Composition Analyzer (Echo
131 Medical Systems, Houston, USA) was used for longitudinal body composition
132 analyses. Mice were scanned twice weekly for the 6-week duration of the
133 succinate water experiments. All body composition analyses were performed in
134 the accompanying EchoMRI software. Mice were weighed on a standard, digital
135 lab scale prior to scanning.

136 **Cell culture**

137 C2C12 cells (ATCC CRL-1772) were grown on tissue culture treated dishes in
138 growth media consisting of high glucose DMEM media supplemented with 10%
139 fetal bovine serum and 1% penicillin/streptomycin. Differentiation-inducing media
140 contains 2% horse serum in place of 10% fetal bovine serum. Differentiating
141 cultures were maintained by alternating fresh media additions and complete
142 media changes on a daily basis for 5 days. DM-succinate (Sigma-Aldrich) was
143 added directly to the culture media upon switching to differentiation media at

144 doses of 4 or 8 mM. Live cell analyses: Cell proliferation and cell death were
145 measured by live cell analysis (Incucyte S3 Live-Cell Imaging System, Essen
146 Bioscience). Percent apoptotic cells over a 48h time course was determined by
147 labeling control or treated cultured C2C12 cells with a phosphatidylserine
148 cyanine fluorescent dye (Annexin V Red Reagent, Essen Bioscience) according
149 to the manufacturer.

150 **Immunostaining**

151 Tissue for immunostaining was placed in a sucrose sink (30%) overnight prior to
152 freezing and sectioning. Sections (8-10 um) were post-fixed in 4%
153 paraformaldehyde (PFA) for 5 minutes at room temperature prior to
154 immunostaining. Once fixed, tissue sections were permeabilized with 0.5%
155 Triton-X100 in PBS followed by blocking with 3% BSA, 0.2% Triton-X and 0.2%
156 Tween-20 in PBS. Primary antibody incubations occurred at RT for 90 minutes
157 followed by incubation with secondary antibody at RT for 30 minutes in buffer
158 described above. The following antibodies were used in this study: MF-20
159 (Developmental Hybridoma Bank), Laminin (Sigma 4HB-2), and BF-F3
160 (Developmental Hybridoma Bank), and SC-71 (Developmental Hybridoma Bank),
161 Pax7 (Developmental Hybridoma Bank), Ki67 (Santa Cruz) and Myogenin (Santa
162 Cruz). Secondary antibodies were all Alexa fluorescent conjugates (488, 555, or
163 647) from Invitrogen or Jackson ImmunoResearch.

164 **Flow cytometry**

165 OPP assay: C2C12 myoblasts were grown to 60% confluency prior to treatment
166 with either control media or 8 mM succinate media for 48 hours. N= 3 plates
167 control, n=3 8mM succinate. Cells were incubated with O-Propargyl-Puromycin
168 (OPP) for 1.5 hours and then trypsinized and stained following the
169 manufacturer's instructions (protein synthesis assay kit (Cayman Chemical
170 #601100)). Viobility 405/452 fixable dye (Miltenyi Biotec 130-110-205) was used
171 as live/dead discriminator. After staining, cells were immediately analyzed by flow
172 cytometry on a MACSquant 10 analyzer (Miltenyi Biotec). Data were analyzed
173 using MACSquantify software (Miltenyi Biotec).

174 **Quantitative RT-qPCR**

175 C2C12 cells were differentiated as described above and cell pellets were
176 collected at each day post differentiation as well as prior to differentiation (day 0,
177 growth media). RNA was isolated using column purification (Qiagen) and cDNA
178 was prepared using high capacity cDNA reverse transcription kit (Applied
179 Biosystems). qPCR was preformed using BioRad CFX384 Real Time System.
180 Primer sequences are available upon request.

181 **Metabolic Assays**

182 A Seahorse XFe24 Analyzer (Agilent) was used to perform mitochondria stress
183 tests and energy phenotyping tests on C2C12 cells. Cells were treated with 4 or
184 8mM DM-succinate or control growth media for 16-18 hours prior to the assay.
185 DM-succinate treatment was maintained throughout the assay. Oligomycin (1
186 μM), FCCP (0.4 μM) and rotenone/antimycin A (1 μM, 1 μM) were used to inhibit
187 mitochondria complexes involved in electron transport/ATP production. Prior to
188 start of the assay, total cells/well counts were obtained on a Celigo imaging
189 cytometer (Nexcelom Bioscience) using Hoechst 33342 stain (Thermofisher). All
190 data were normalized to Celigo counts of cells/well. Wave software (Agilent,
191 version 3.0.11) was used in the analysis of energy phenotyping data.

192 **Quantitative metabolite analyses**

193 Sample preparation: Cells were treated for 48 hours with 4 or 8 mM DM-
194 succinate, washed 3 times with PBS, and stored at -80C until metabolite
195 extraction. Muscle tissue was cut into ~50 mg pieces, flash frozen in liquid
196 nitrogen, and stored at -80 C until metabolite extraction. Conditioned media was
197 flash frozen in liquid nitrogen. All samples were submitted to the Mayo Clinic
198 Metabolomics Resource Core for targeted metabolomics.

199 TCA: Concentration of TCA analytes were measured by gas chromatograph
200 mass spectrometry (GC/MS) as previously described with a few modifications[39].
201 Briefly, cell culture supernatants were spiked with internal solutions containing U-
202 ^{13}C labeled analytes. Proteins were removed by adding 250 ul of chilled

203 methanol and acetonitrile solution to the sample mixture. After drying the
204 supernatant in the speed vac, the sample was derivatized with ethoxime and
205 then with MtBSTFA + 1% tBDMCS (N-Methyl-N-(t-Butyldimethylsilyl)-
206 Trifluoroacetamide + 1% t-Butyldimethylchlorosilane) before it was analyzed on
207 an Agilent 5975C GC/MS (gas chromatography/mass spectrometry) under
208 electron impact and single ion monitoring conditions. Concentrations of lactic
209 acid (m/z 261.2), fummaric acid (m/z 287.1), succinic acid (m/z 289.1),
210 oxaloacetic acid (m/z 346.2), ketoglutaric acid (m/z 360.2), malic acid (m/z
211 419.3), aspartic acid (m/z 418.2), 2-hydroxyglutaratic acid (m/z 433.2), cis-
212 aconitic acid (m/z459.3), citric acid (m/z 591.4), and isocitric acid (m/z 591.4),
213 glutamic acid (m/z 432.4) were measured against a 7-point calibration curves
214 that underwent the same derivatization. n=1 for each supernatant sample, which
215 was run in 2 technical replicates after derivatization.

216 **Untargeted metabolomics analyses**

217 Three biological replicates of control and DM-succinate (8 mM) treated C2C12
218 cells were prepared for untargeted metabolomics analyses as follows: cells were
219 grown to 60% confluency and then treated with 8 mM succinate for 48 hours, at
220 which time plates were washed with PBS and cells were scraped and pelleted,
221 followed by storage at -80° C. Samples were submitted to the Metabolomics
222 Core at Mayo Clinic (Rochester, MN, USA) for metabolomics profiling by liquid
223 chromatography-mass spectrometry (LC/MS) using 6550 iFunnel Quadrupole
224 Time of Flight (Q-TOF) mass spectrometer (Agilent). Metabolites were then
225 identified using METLIN database with Mass Profiler Professional software
226 (Agilent). Annotated metabolites with a p value less than 0.05 and a fold change
227 greater than 2 were further analyzed using MetaboAnalyst network explorer[40]
228 (metabolite-metabolite interactions) and enrichment analysis (pathway
229 associated metabolite sets) tools. KEGG and HMDB identifiers were used in
230 MetaboAnalyst.

231 **RNA sequencing analysis**

232 Sample/library preparation: Three biological replicates of control and DM-
233 succinate (8mM) treated C2C12 cells were prepared for RNA sequencing
234 analyses as follows: cells were grown to 60% confluency and then treated with
235 8mM succinate for 48 hours, at which time plates were washed with PBS and
236 cells were scraped and pelleted, followed by storage at -80° C. Frozen cell
237 pellets were submitted to the Mayo Clinic Medical Genome Facility where RNA
238 quality was determined using the Fragment Analyzer from AATI. RNA samples
239 that have RQN values ≥6 were approved for library prep and sequencing. RNA
240 libraries were prepared using 200 ng of good quality total RNA according to the
241 manufacturer's instructions for the TruSeq RNA Sample Prep Kit v2 (Illumina,
242 San Diego, CA), employing poly-A mRNA enrichment using oligo dT magnetic
243 beads. The final adapter-modified cDNA fragments were enriched by 12 cycles of
244 PCR using Illumina TruSeq PCR primers. The concentration and size
245 distribution of the completed libraries were determined using a Fragment
246 Analyzer (AATI, Ankeny, IA) and Qubit fluorometry (Invitrogen, Carlsbad, CA).
247 Libraries were sequenced following Illumina's standard protocol using the
248 Illumina cBot and HiSeq 3000/4000 PE Cluster Kit, yielding approximately 48-70
249 million fragment reads per sample. The flow cells were sequenced as 100 X 2
250 paired end reads on an Illumina HiSeq 4000 using HiSeq 3000/4000 sequencing
251 kit and HCS v3.3.52 collection software. Base-calling was performed using
252 Illumina's RTA version 2.7.3. Bioinformatics/Data Processing: All bioinformatics
253 analyses were done through the Mayo Clinic Bioinformatics Core. The raw RNA
254 sequencing paired-end reads for the samples were processed through the Mayo
255 RNA-Seq bioinformatics pipeline, MAP-RSeq version 3.0.0[41]. Briefly, MAP-RSeq
256 employs the splice-aware aligner, STAR[42], to align reads to the reference mouse
257 genome build mm10. Gene and exon expression quantification were performed
258 using the Subread[43] package to obtain both raw and normalized (RPKM – Reads
259 Per Kilobase per Million mapped reads) reads.

260 **Statistics**

261 Data are represented as the mean ± SD using GraphPad Prism unless noted
262 otherwise in the figure legends. Quantification of nuclei per MyHC+ structure was
263 analyzed using nonparametric, Mann-Whitney t-tests. Quantification of muscle
264 cross sections using minimum feret diameter measurements was analyzed by
265 non-linear regression (gaussian, least squares method) and compared between
266 conditions using an extra sum-of-squares F test. All other comparisons between
267 groups were performed using unpaired two-tailed student's t tests or multiple t
268 tests with Holm-Sidak multiple testing correction, as noted in figure legends. For
269 all analyses, a $p<0.05$ was considered significant (denoted with *); a $p<0.01$ was
270 denoted with ** unless noted otherwise in the figure legend.

271 **Data availability**

272 The RNAseq dataset generated and analyzed during the current study is
273 available in the Sequence Read Archive (SRA) (National Center for
274 Biotechnology Information, NCBI), submission number SUB6936750, BioProject
275 ID PRJNA605465. All other datasets generated during the current study are
276 available from the corresponding author upon request.
277

278 **RESULTS**

279 Modeling succinate accumulation and evaluating consequences on growth and
280 atrophy

281 To evaluate the effects of succinate on *in vitro* myoblast function, we first
282 sought to adapt an established paradigm of intracellular succinate accumulation
283 for use in myoblast cells. Succinate has very low cell permeability *in vitro*, so we
284 began our studies using dimethyl-succinate (DM-succinate or DMS), a cell
285 permeable succinate analog used in prior studies to elevate intracellular
286 metabolite levels[18,19]. We treated proliferating C2C12 myoblasts for 48 hours with
287 two concentrations of DM-succinate, 4 mM and 8 mM, and then performed
288 targeted metabolomics to quantify levels of TCA cycle-associated metabolites.
289 We found that 8 mM DM-succinate treatment resulted in a significant increase in
290 intracellular succinate (~2.5-fold) compared to control treatment, similar in
291 magnitude to previously reported values[18] and consistent with the degree of
292 succinate accumulation in wasting cancer patients[17]. We did not detect
293 statistically significant changes in most other TCA metabolites analyzed, with the
294 exception of small (<2 fold) but significant increases in malate and glutamate
295 (**Fig. 1A**). We chose to evaluate this dosing paradigm further to investigate the
296 effects of intracellular succinate elevation on myogenesis. Cell proliferation and
297 apoptosis are important regulators of myogenesis. To test if succinate would
298 influence either of these processes, we evaluated cells treated with three doses
299 of DM-succinate over 48 hours. We did not see significant differences in
300 proliferation over this time period, and only saw increased apoptosis rates with
301 16 mM DM-succinate treatment (**Fig. 1B, C**).

302 A major feature of cancer-associated muscle wasting is myofiber atrophy due
303 to either enhanced protein catabolism or impaired protein anabolism. In
304 myoblasts exposed to DM-succinate, we did not observe an increase in mRNA
305 transcripts encoding for E3 ubiquitin ligases (MuRF1, Atrogin-1) typically
306 associated with enhanced muscle catabolism (**Fig. 1D**). We did, however,
307 observe a reduction in protein anabolism as determined by an O-propargyl-

308 puromycin (OPP) incorporation assay, performed in proliferating C2C12
309 myoblasts treated with 8 mM DM-succinate for 48 hours (**Fig. 1E**). Interestingly,
310 differentiated C2C12 myotubes treated with 8 mM DM-succinate for 24 hours
311 post myogenic differentiation did not exhibit statistically significant alterations in
312 mean myotube diameter (**Fig. 1F**), suggesting that the DM-succinate-associated
313 protein anabolism deficits are not sufficient to drive muscle atrophy.

314 Elevated succinate levels impair *in vitro* myogenesis

315 To gain a more comprehensive understanding of the molecular changes
316 associated with succinate elevation, we performed RNA sequencing (RNA-seq)
317 on proliferating C2C12 myoblasts treated with 8 mM DM-succinate for 48 hours.
318 Analysis of the transcripts involved in myogenesis and lineage specification
319 revealed widespread transcript down-regulation after exposure to DM-succinate
320 (**Fig. 2A**). These results led us to more closely investigate myogenic progression
321 by differentiating C2C12 myoblast cultures in low serum conditions for 5 days in
322 the presence or absence of 8 mM DM-succinate. In this assay, we assessed the
323 degree of terminal differentiation by quantitative RT-PCR analysis of myogenic
324 transcript expression (Pax7, MyoD1, Myog, and MyH1) and the number of nuclei
325 fused into differentiated, Myosin Heavy Chain-positive myocytes/myotubes.
326 Analysis of key myogenic transcript expression patterns supported the RNA-seq
327 data, showing downregulation of MyoD1, Myog and MyH1, particularly earlier in
328 the differentiation time course (**Fig. 2B**). Although not statistically significant,
329 Pax7 expression was trending upwards in DM-succinate-treated cells (**Fig. 2B**).
330 Differentiating C2C12 cells in the presence of 8 mM DM-succinate resulted in an
331 impaired ability to form mature, multinucleated Myosin Heavy Chain-positive
332 structures (control, 4 mM DM-succinate, 8 mM DM-succinate mean
333 nuclei/myotube values = 5.43, 4.62, 2.98, respectively; **Fig. 2C, D**). Together,
334 these data show that elevated succinate in muscle cells influences protein
335 anabolism and suppresses myogenic differentiation and that these changes are
336 distinct from direct myotube atrophy via enhanced protein catabolism.

337 *In vivo* succinate supplementation impairs skeletal muscle homeostasis

338 Defects in progenitor cell activation, expansion, differentiation, or fusion
339 compromise the regenerative capacity of skeletal muscle. Given our observations
340 that DM-succinate impairs myogenic differentiation *in vitro*, we next asked if
341 succinate supplementation negatively impacts *in vivo* skeletal muscle
342 homeostasis. Wildtype mice were either supplemented with vehicle (1% sucrose)
343 control drinking water or water with 2% succinate (+1% sucrose vehicle). We
344 found that there was no significant difference in total body weight across the
345 supplementation, or at the endpoint (**Fig. 3A, B**). In addition to total body weight,
346 we longitudinally monitored body composition of the mice twice weekly for six
347 weeks using echo magnetic resonance imaging (echoMRI). Total lean mass, as
348 measured by echoMRI-based body composition analyses, did not show a
349 difference between vehicle and succinate-supplemented mice (**Fig. 3C)**.
350 Comparisons of *tibialis anterior* (TA) and *gastrocnemius* (GR) muscle wet
351 weights after six weeks of supplementation did not reveal significant differences
352 between experimental groups (**Fig. 3D)**. Following six weeks of succinate
353 supplementation, we harvested TA muscles and stained tissue cross sections
354 with laminin, a protein on the myofiber membrane, to evaluate myofiber size (**Fig.**
355 **3E)**. We quantified myofiber minimum feret diameters using Myovision[44] and
356 found a statistically significant ($p<0.0001$) decrease (~6%) in the mean of non-
357 linear regressions fit to the histograms of minimum feret diameter distribution
358 between control and succinate supplemented cohorts (**Fig. 3F, Supplementary**
359 **Fig S1A, B)**.

360 <u>Succinate supplementation impairs skeletal muscle regeneration</u>

361 Muscle progenitor cells are required for efficient muscle regeneration
362 following serious injury[23-25]. In order to challenge resident satellite cells
363 chronically exposed to elevated succinate, after six weeks of supplementation,
364 we injured TA muscles with intramuscular barium chloride injection (1.2%). At 7
365 days and 28 days post injury (dpi) we harvested TA muscle for histological
366 analysis. At 7 dpi, we observed statistically significant ($p=0.0006$) differences in
367 myofiber regeneration as evidenced by ~16% reduction in the mean of non-linear
368 regression curves fit to the minimum feret diameter distribution (**Fig. 4A, B,**

369 **Supplementary Figure S1C, D**). Muscle regeneration post barium chloride injury
370 is typically completed four weeks post injury in healthy, adult mice. When we
371 analyzed minimum feret diameters at 28 dpi, the difference in the mean of non-
372 linear regression curves fit to the minimum feret diameter distribution became
373 more pronounced (~48% reduction, $p<0.0001$) (**Fig. 4C, D, Supplementary**
374 **Figure S1E, F**). Injured TA muscle in succinate supplemented mice exhibited
375 large areas of poorly regenerated tissue (**Fig. 4C**). To further investigate the
376 impacts of chronic succinate supplementation on the satellite cell population we
377 looked at markers of myogenic differentiation and proliferation. We saw no
378 significant difference in the number of total (PAX7+) or proliferating
379 (PAX7+KI67+) muscle progenitor cells in succinate-supplemented animals at 7-
380 or 28 dpi, in concordance with *in vitro* proliferation data (**Fig. 4E, F; top**). At 7-
381 days post injury there was no difference in the number of MYOG+ differentiating
382 muscle progenitor cells between succinate- and vehicle-supplemented mice.
383 However, we did see a significant accumulation of differentiating muscle
384 progenitor cells (MYOG+) in succinate-supplemented animals at 28 dpi,
385 indicative of stalled or incomplete myogenesis. In comparison, vehicle-
386 supplemented mice had low numbers of MYOG+ cells at 28 dpi likely due to
387 effective completion of myogenesis (**Fig. 4E; bottom**). Taken together, these
388 data show that succinate supplementation alters progenitor cell dynamics
389 resulting in impaired skeletal muscle homeostasis and diminished skeletal
390 muscle regeneration.

391 <u>Succinate elevation disrupts multiple metabolic networks in muscle cells</u>

392 Succinate is gaining traction as a metabolite capable of acting as more than a
393 substrate for succinate dehydrogenase and the respiratory chain[45]. Notably,
394 succinate is located at the intersection of many diverse metabolic pathways and
395 can influence a wide range of metabolic processes[46,47]. We performed non-
396 targeted metabolomics profiling on control and 8 mM treated (48h) C2C12
397 myoblasts and found a striking number of differentially abundant metabolites
398 (DAMs) between in the two conditions (214 features with $p<0.05$, FC>2). Network
399 analyses of metabolic pathways associated with these DAMs implicated

400 pathways involved in amino acid and nucleotide metabolism, as well as
401 metabolic processes associated with mitochondrial metabolism and the TCA
402 cycle (**Fig. 5A,B**). Considering the central role of the mitochondria in coordinating
403 cellular metabolism and the known involvement of succinate in several
404 mitochondria-coupled processes, we posited that succinate elevation could result
405 in mitochondria dysfunction. Prior evidence suggests that myogenic
406 differentiation involves metabolic rewiring characterized by increased
407 mitochondria mass and a shift towards oxidative phosphorylation[48,49]. To assess
408 mitochondria function, we measured cellular oxygen consumption rates (OCR) in
409 proliferating myoblasts treated with 4 mM and 8 mM DM-succinate exposed to
410 mitochondrial stressors. When treated with compounds targeting ATP synthase
411 (oligomycin), the hydrogen ion gradient (FCCP), and complex I/III
412 (Rotenone/Antimycin A), we noted altered OCR dynamics in myoblasts treated
413 with the highest dose (8 mM) of DM-succinate (**Fig. 5C**). Maximal respiration, as
414 determined by OCR measurements following the addition of the ionophore
415 FCCP, was significantly reduced (~35%) in the presence of 8 mM DM-succinate
416 (**Fig. 5D**), thus significantly decreasing mitochondria reserve capacity[50] (~50%
417 reduction; **Fig. 5E**). Basal respiration rates, and non-mitochondrial respiration
418 were unaffected by succinate elevation (**Fig. 5F, G**). The ability of cells to
419 respond to general mitochondrial stress was further assessed using an energy
420 phenotyping test, which exposes cells to FCCP and oligomycin simultaneously
421 and measures both ECAR (extracellular acidification rate) and OCR. When
422 stressed, control cells exhibited expected increases in ECAR and OCR, whereas
423 DM-succinate treated cells responded poorly (**Fig. 5H**). Taken together, these
424 data show that while elevated succinate does not grossly affect mitochondria
425 morphology or basal (resting) respiration parameters, it does impact the ability of
426 cells to maximally engage mitochondrial respiration under stressful conditions.

427 **DISCUSSION**

428 Mitochondria and tricarboxylic acid (TCA) cycle defects are commonly
429 observed in wasting skeletal muscle[51-53]. Direct alterations to TCA metabolite
430 stoichiometry could therefore, in principal, contribute to functional deficits
431 associated with muscle wasting. Indeed, multiple studies show that perturbations
432 in the succinate/alpha-ketoglutarate ratio underlie a spectrum of cellular defects
433 ranging from epigenome alterations to mitochondria deficits[15,19,54]. In this study,
434 we found that succinate elevation in muscle progenitor cells impaired myogenic
435 differentiation *in vitro* and disrupted *in vivo* muscle regeneration in response to
436 injury. While this study did not directly assess the role of muscle progenitor cells
437 in cancer-associated cachexia, we provide proof-of-concept evidence that tumor-
438 associated factors (ie. succinate) are capable of functionally perturbing
439 myogenesis, a process implicated by several groups as a contributing factor to
440 muscle wasting[6,27,30,35,38]. We anticipate that future identification and evaluation
441 of other tumor-associated metabolites will reveal many new drivers of muscle
442 wasting and will prompt a re-evaluation of therapeutic strategies designed to limit
443 cancer-associated weight loss.

444 Several groups show that elevated succinate can influence multiple metabolic
445 processes including NADH/NAD+ redox state, phosphate metabolism, carbon
446 source utilization, amino acid incorporation, and fatty acid synthesis[46,47,55,56]. Of
447 note, succinate CoA ligase (SUCL) – which catalyzes succinyl-CoA and
448 ADP/GDP to CoASH, succinate, and ATP/GTP – is subject to inhibition by the
449 accumulation succinate[45]. This product inhibition of SUCL could lead to a buildup
450 of upstream CoA species such as propionyl-CoA and methylmalonyl-CoA, which
451 in turn would likely inhibit the catabolism of many macromolecules that are
452 normally metabolized to succinyl-CoA, including branched-chain amino acids,
453 cholesterol, propionate, and odd-chain fatty acids[57,58]. Future studies focusing on
454 how succinate engages other metabolic networks will help to clarify how elevated
455 succinate levels result in impaired muscle repair/regeneration.

456 Recent work shows that mitochondria and energy homeostasis play important
457 roles in the regulation of myogenesis. A study that measured the relative
458 contribution of oxidative phosphorylation (OXPHOS) to total cellular ATP in
459 muscle cells demonstrates a shift from ~30% OXPHOS dependent ATP
460 production in proliferating myoblasts to ~60% in terminally differentiated
461 myotubes[59]. Accordingly, mRNA expression profiles and activities of
462 mitochondrial enzymes including citrate synthase, isocitrate dehydrogenase, 3-
463 hydroxyacyl-CoA dehydrogenase, cytochrome oxidase, NADH dehydrogenase,
464 and succinate dehydrogenase are markedly increased during myogenic
465 differentiation[60]. Several lines of evidence show that functional impairment of
466 mitochondria negatively regulates myogenic differentiation. First, mitochondrial
467 protein synthesis inhibition by chloramphenicol impaired chick embryo myoblast
468 fusion, even when proliferation/apoptosis rates were maintained by tryptose
469 phosphate broth or nucleoside supplementation[61]. Second, over-expression of
470 key factors involved in mitochondria biogenesis (PGC-1 genes) in skeletal
471 muscle enhanced mtDNA content, mitochondrial enzyme activities, and exercise
472 performance[62], whereas mice lacking PGC-1 show reduced mitochondria
473 numbers, decreased expression of mitochondrial genes, and diminished muscle
474 function[63,64]. We found that while DM-succinate impaired the maximal respiratory
475 capacity of myoblasts, DM-succinate failed to affect basal mitochondria
476 bioenergetics parameters or gross mitochondria morphology. Accordingly,
477 proliferation and apoptosis rates were unchanged in DM-succinate treated cells.
478 These data support the hypothesis that elevated succinate levels specifically
479 impair myogenic differentiation, an energetically demanding process that
480 challenges myoblast mitochondria.

481 Our data show that *in vivo* succinate supplementation impairs muscle
482 morphometric parameters and regeneration properties, thus adding to the
483 growing list of studies that report metabolite-driven skeletal muscle mass and/or
484 functional alterations[65,66]. Cancer-associated lean mass loss is considered a
485 metabolic disorder with complex and overlapping mechanisms of action
486 (including both increased catabolism and impaired regeneration) that ultimately

487 lead to a decline in skeletal muscle mass and function. While cytokines and
488 chemokines have garnered the most attention as drivers of muscle wasting
489 phenotypes, efforts to target, block or neutralize specific wasting factors have
490 seen little success[67-69]. Our data underscore the importance of metabolites as
491 regulators of muscle progenitor cell function, bringing attention to an
492 understudied therapeutic avenue.

ACKNOWLEDGEMENTS

The authors wish to thank members of the Doles lab for helpful discussions and manuscript suggestions and the Mayo Microscopy and Cell Analysis Core for experimental and technical support. J.D. was supported by the National Institutes of Health/National Institute of Arthritis, Musculoskeletal and Skin Diseases (NIH/NIAMS) R00AR66696, Mayo Clinic start-up funds, Career Development Awards from the Mayo Clinic SPORE in Pancreatic Cancer (NIH/ National Cancer Institute (NCI) CA102701) and the American Association for Cancer Research/Pancreatic Cancer Action Network, and the Glenn Foundation for Medical Research. P.C.A was supported by the Mayo Clinic Regenerative Sciences Training Program (RSTP). Metabolomics studies were made possible by the Mayo Clinic Metabolomics Resource Core through NIH/National Institute of Diabetes and Digestive and Kidney Disease (NIDDK) U24DK10049 originating from the NIH Director's Common Fund. The authors of this manuscript certify that they comply with the ethical guidelines for authorship and publishing in the Journal of Cachexia, Sarcopenia and Muscle[70].

509 **AUTHOR CONTRIBUTIONS**

510 Study design: PCA, KAH, JDD. Data collection: PCA, KAH, AS, AMS. Data
511 analysis/interpretation: PCA, KAH, JDD. Writing and editing of manuscript: PCA,
512 KAH, AJ, JDD. All authors approved this manuscript.

COMPETING INTERESTS STATEMENT

The authors have no competing interests to declare.

515 **REFERENCES**

516 1 Zhou, X. *et al.* Reversal of cancer cachexia and muscle wasting by
517 ActRIIB antagonism leads to prolonged survival. *Cell* **142**, 531-543,
518 doi:10.1016/j.cell.2010.07.011 (2010).
519 2 Toledo, M. *et al.* Complete reversal of muscle wasting in experimental
520 cancer cachexia: Additive effects of activin type II receptor inhibition and
521 β-2 agonist. *Int J Cancer* **138**, 2021-2029, doi:10.1002/ijc.29930 (2016).
522 3 Pal, M., Febbraio, M. A. & Whitham, M. From cytokine to myokine: the
523 emerging role of interleukin-6 in metabolic regulation. *Immunol Cell Biol*
524 **92**, 331-339, doi:10.1038/icb.2014.16 (2014).
525 4 Onesti, J. K. & Guttridge, D. C. Inflammation based regulation of cancer
526 cachexia. *Biomed Res Int* **2014**, 168407, doi:10.1155/2014/168407
527 (2014).
528 5 Loumaye, A. *et al.* Role of Activin A and myostatin in human cancer
529 cachexia. *J Clin Endocrinol Metab* **100**, 2030-2038, doi:10.1210/jc.2014-
530 4318 (2015).
531 6 Hogan, K. A. *et al.* Tumor-derived cytokines impair myogenesis and alter
532 the skeletal muscle immune microenvironment. *Cytokine*,
533 doi:10.1016/j.cyto.2017.11.006 (2017).
534 7 VanderVeen, B. N., Fix, D. K. & Carson, J. A. Disrupted Skeletal Muscle
535 Mitochondrial Dynamics, Mitophagy, and Biogenesis during Cancer
536 Cachexia: A Role for Inflammation. *Oxid Med Cell Longev* **2017**, 3292087,
537 doi:10.1155/2017/3292087 (2017).
538 8 Carson, J. A., Hardee, J. P. & VanderVeen, B. N. The emerging role of
539 skeletal muscle oxidative metabolism as a biological target and cellular
540 regulator of cancer-induced muscle wasting. *Semin Cell Dev Biol* **54**, 53-
541 67, doi:10.1016/j.semcdb.2015.11.005 (2016).
542 9 Romanello, V. *et al.* Mitochondrial fission and remodelling contributes to
543 muscle atrophy. *EMBO J* **29**, 1774-1785, doi:10.1038/emboj.2010.60
544 (2010).
545 10 Wu, S., Zhou, F., Zhang, Z. & Xing, D. Mitochondrial oxidative stress
546 causes mitochondrial fragmentation via differential modulation of
547 mitochondrial fission-fusion proteins. *FEBS J* **278**, 941-954,
548 doi:10.1111/j.1742-4658.2011.08010.x (2011).
549 11 Bordi, M., Nazio, F. & Campello, S. The Close Interconnection between
550 Mitochondrial Dynamics and Mitophagy in Cancer. *Front Oncol* **7**, 81,
551 doi:10.3389/fonc.2017.00081 (2017).
552 12 Julienne, C. M. *et al.* Cancer cachexia is associated with a decrease in
553 skeletal muscle mitochondrial oxidative capacities without alteration of
554 ATP production efficiency. *J Cachexia Sarcopenia Muscle* **3**, 265-275,
555 doi:10.1007/s13539-012-0071-9 (2012).
556 13 Tannahill, G. M. *et al.* Succinate is an inflammatory signal that induces IL-
557 1β through HIF-1α. *Nature* **496**, 238-242, doi:10.1038/nature11986
558 (2013).

559 14 Selak, M. A. *et al.* Succinate links TCA cycle dysfunction to oncogenesis
560 by inhibiting HIF-alpha prolyl hydroxylase. *Cancer Cell* **7**, 77-85,
561 doi:10.1016/j.ccr.2004.11.022 (2005).
562 15 Xiao, M. *et al.* Inhibition of α-KG-dependent histone and DNA
563 demethylases by fumarate and succinate that are accumulated in
564 mutations of FH and SDH tumor suppressors. *Genes Dev* **26**, 1326-1338,
565 doi:10.1101/gad.191056.112 (2012).
566 16 Park, J. *et al.* SIRT5-mediated lysine desuccinylation impacts diverse
567 metabolic pathways. *Mol Cell* **50**, 919-930,
568 doi:10.1016/j.molcel.2013.06.001 (2013).
569 17 Yang, Q.-J. *et al.* Serum and urine metabolomics study reveals a distinct
570 diagnostic model for cancer cachexia. *J Cachexia Sarcopenia Muscle* **9**,
571 71-85, doi:10.1002/jcsm.12246 (2018).
572 18 TeSlaa, T. *et al.* α-Ketoglutarate Accelerates the Initial Differentiation of
573 Primed Human Pluripotent Stem Cells. *Cell Metab* **24**, 485-493,
574 doi:10.1016/j.cmet.2016.07.002 (2016).
575 19 Carey, B. W., Finley, L. W. S., Cross, J. R., Allis, C. D. & Thompson, C. B.
576 Intracellular α-ketoglutarate maintains the pluripotency of embryonic stem
577 cells. *Nature* **518**, 413-416, doi:10.1038/nature13981 (2015).
578 20 Talbert, E. E. & Guttridge, D. C. Impaired regeneration: A role for the
579 muscle microenvironment in cancer cachexia. *Semin Cell Dev Biol* **54**, 82-
580 91, doi:10.1016/j.semcdb.2015.09.009 (2016).
581 21 Pawlikowski, B., Pulliam, C., Betta, N. D., Kardon, G. & Olwin, B. B.
582 Pervasive satellite cell contribution to uninjured adult muscle fibers. *Skelet*
583 *Muscle* **5**, 42, doi:10.1186/s13395-015-0067-1 (2015).
584 22 Keefe, A. C. *et al.* Muscle stem cells contribute to myofibres in sedentary
585 adult mice. *Nat Commun* **6**, 7087, doi:10.1038/ncomms8087 (2015).
586 23 Murphy, M. M., Lawson, J. A., Mathew, S. J., Hutcheson, D. A. & Kardon,
587 G. Satellite cells, connective tissue fibroblasts and their interactions are
588 crucial for muscle regeneration. *Development* **138**, 3625-3637,
589 doi:10.1242/dev.064162 (2011).
590 24 Lepper, C., Partridge, T. A. & Fan, C.-M. An absolute requirement for
591 Pax7-positive satellite cells in acute injury-induced skeletal muscle
592 regeneration. *Development* **138**, 3639-3646, doi:10.1242/dev.067595
593 (2011).
594 25 Sambasivan, R. *et al.* Pax7-expressing satellite cells are indispensable for
595 adult skeletal muscle regeneration. *Development* **138**, 3647-3656,
596 doi:10.1242/dev.067587 (2011).
597 26 Mozdziak, P. E., Pulvermacher, P. M. & Schultz, E. Muscle regeneration
598 during hindlimb unloading results in a reduction in muscle size after
599 reloading. *J Appl Physiol (1985)* **91**, 183-190,
600 doi:10.1152/jappl.2001.91.1.183 (2001).
601 27 Mitchell, P. O. & Pavlath, G. K. Skeletal muscle atrophy leads to loss and
602 dysfunction of muscle precursor cells. *Am J Physiol Cell Physiol* **287**,
603 C1753-1762, doi:10.1152/ajpcell.00292.2004 (2004).

604 28 Viguie, C. A., Lu, D. X., Huang, S. K., Rengen, H. & Carlson, B. M.
605 Quantitative study of the effects of long-term denervation on the extensor
606 digitorum longus muscle of the rat. *Anat Rec* **248**, 346-354 (1997).
607 29 Liao, H. *et al.* [Pax7 and depletion of satellite cell pool in prolonged
608 denervated skeletal muscles of adult rats]. *Zhongguo Xiu Fu Chong Jian*
609 *Wai Ke Za Zhi* **23**, 92-96 (2009).
610 30 Langen, R. C. J. *et al.* Muscle wasting and impaired muscle regeneration
611 in a murine model of chronic pulmonary inflammation. *Am J Respir Cell*
612 *Mol Biol* **35**, 689-696, doi:10.1165/rcmb.2006-0103OC (2006).
613 31 Wu, X., Walters, T. J. & Rathbone, C. R. Skeletal muscle satellite cell
614 activation following cutaneous burn in rats. *Burns* **39**, 736-744,
615 doi:10.1016/j.burns.2012.10.016 (2013).
616 32 Corrick, K. L. *et al.* Serum from human burn victims impairs myogenesis
617 and protein synthesis in primary myoblasts. *Front Physiol* **6**, 184,
618 doi:10.3389/fphys.2015.00184 (2015).
619 33 Aragno, M. *et al.* Oxidative stress impairs skeletal muscle repair in diabetic
620 rats. *Diabetes* **53**, 1082-1088 (2004).
621 34 Krause, M. P., Moradi, J., Nissar, A. A., Riddell, M. C. & Hawke, T. J.
622 Inhibition of plasminogen activator inhibitor-1 restores skeletal muscle
623 regeneration in untreated type 1 diabetic mice. *Diabetes* **60**, 1964-1972,
624 doi:10.2337/db11-0007 (2011).
625 35 Zhang, L., Wang, X. H., Wang, H., Du, J. & Mitch, W. E. Satellite cell
626 dysfunction and impaired IGF-1 signaling cause CKD-induced muscle
627 atrophy. *J Am Soc Nephrol* **21**, 419-427, doi:10.1681/ASN.2009060571
628 (2010).
629 36 Dasarathy, S. Cause and management of muscle wasting in chronic liver
630 disease. *Curr Opin Gastroenterol* **32**, 159-165,
631 doi:10.1097/MOG.0000000000000261 (2016).
632 37 Mehl, K. A., Davis, J. M., Berger, F. G. & Carson, J. A. Myofiber
633 degeneration/regeneration is induced in the cachectic ApcMin/+ mouse. *J*
634 *Appl Physiol (1985)* **99**, 2379-2387, doi:10.1152/japplphysiol.00778.2005
635 (2005).
636 38 He, W. A. *et al.* NF-κB-mediated Pax7 dysregulation in the muscle
637 microenvironment promotes cancer cachexia. *J Clin Invest* **123**, 4821-
638 4835, doi:10.1172/JCI68523 (2013).
639 39 Dutta, T. *et al.* Impact of Long-Term Poor and Good Glycemic Control on
640 Metabolomics Alterations in Type 1 Diabetic People. *J Clin Endocrinol*
641 *Metab* **101**, 1023-1033, doi:10.1210/jc.2015-2640 (2016).
642 40 Chong, J. *et al.* MetaboAnalyst 4.0: towards more transparent and
643 integrative metabolomics analysis. *Nucleic Acids Res* **46**, W486-W494,
644 doi:10.1093/nar/gky310 (2018).
645 41 Kalari, K. R. *et al.* MAP-RSeq: Mayo Analysis Pipeline for RNA
646 sequencing. *BMC Bioinformatics* **15**, 224, doi:10.1186/1471-2105-15-224
647 (2014).
648 42 Dobin, A. *et al.* STAR: ultrafast universal RNA-seq aligner. *Bioinformatics*
649 **29**, 15-21, doi:10.1093/bioinformatics/bts635 (2013).

43 Liao, Y., Smyth, G. K. & Shi, W. The Subread aligner: fast, accurate and scalable read mapping by seed-and-vote. *Nucleic Acids Res* **41**, e108, doi:10.1093/nar/gkt214 (2013).

44 Wen, Y. *et al.* MyoVision: software for automated high-content analysis of skeletal muscle immunohistochemistry. *J Appl Physiol (1985)* **124**, 40-51, doi:10.1152/japplphysiol.00762.2017 (2018).

45 Tretter, L., Patocs, A. & Chinopoulos, C. Succinate, an intermediate in metabolism, signal transduction, ROS, hypoxia, and tumorigenesis. *Biochim Biophys Acta* **1857**, 1086-1101, doi:10.1016/j.bbabio.2016.03.012 (2016).

46 Stovell, M. G. *et al.* The effect of succinate on brain NADH/NAD(+) redox state and high energy phosphate metabolism in acute traumatic brain injury. *Sci Rep* **8**, 11140, doi:10.1038/s41598-018-29255-3 (2018).

47 Aspuria, P. P. *et al.* Succinate dehydrogenase inhibition leads to epithelial-mesenchymal transition and reprogrammed carbon metabolism. *Cancer Metab* **2**, 21, doi:10.1186/2049-3002-2-21 (2014).

48 Wagatsuma, A. & Sakuma, K. Mitochondria as a potential regulator of myogenesis. *ScientificWorldJournal* **2013**, 593267, doi:10.1155/2013/593267 (2013).

49 Ryall, J. G. *et al.* The NAD(+)-Dependent SIRT1 Deacetylase Translates a Metabolic Switch into Regulatory Epigenetics in Skeletal Muscle Stem Cells. *Cell Stem Cell* **16**, 171-183, doi:10.1016/j.stem.2014.12.004 (2015).

50 Divakaruni, A. S., Rogers, G. W. & Murphy, A. N. Measuring Mitochondrial Function in Permeabilized Cells Using the Seahorse XF Analyzer or a Clark-Type Oxygen Electrode. *Curr Protoc Toxicol* **60**, 25.22.21-16, doi:10.1002/0471140856.tx2502s60 (2014).

51 Der-Torossian, H. *et al.* Metabolic derangements in the gastrocnemius and the effect of Compound A therapy in a murine model of cancer cachexia. *J Cachexia Sarcopenia Muscle* **4**, 145-155, doi:10.1007/s13539-012-0101-7 (2013).

52 Tzika, A. A. *et al.* Skeletal muscle mitochondrial uncoupling in a murine cancer cachexia model. *Int J Oncol* **43**, 886-894, doi:10.3892/ijo.2013.1998 (2013).

53 Koopman, R., Ly, C. H. & Ryall, J. G. A metabolic link to skeletal muscle wasting and regeneration. *Front Physiol* **5**, 32, doi:10.3389/fphys.2014.00032 (2014).

54 Vatrinet, R. *et al.* The α-ketoglutarate dehydrogenase complex in cancer metabolic plasticity. *Cancer Metab* **5**, 3, doi:10.1186/s40170-017-0165-0 (2017).

55 Whereat, A. F., Hull, F. E. & Orishimo, M. W. The role of succinate in the regulation of fatty acid synthesis by heart mitochondria. *J Biol Chem* **242**, 4013-4022 (1967).

56 Fonnesu, A., Capaccioli, S. & Cini-Neri, G. Effects of succinate on amino acid incorporation into protein during chemical carcinogenesis. *Toxicol Pathol* **12**, 400-403, doi:10.1177/019262338401200416 (1984).

57 Ostergaard, E. Disorders caused by deficiency of succinate-CoA ligase. *J Inherit Metab Dis* **31**, 226-229, doi:10.1007/s10545-008-0828-7 (2008).
58 Kacso, G. *et al.* Two transgenic mouse models for beta-subunit components of succinate-CoA ligase yielding pleiotropic metabolic alterations. *Biochem J* **473**, 3463-3485, doi:10.1042/BCJ20160594 (2016).
59 Leary, S. C., Battersby, B. J., Hansford, R. G. & Moyes, C. D. Interactions between bioenergetics and mitochondrial biogenesis. *Biochim Biophys Acta* **1365**, 522-530 (1998).
60 Moyes, C. D., Mathieu-Costello, O. A., Tsuchiya, N., Filburn, C. & Hansford, R. G. Mitochondrial biogenesis during cellular differentiation. *Am J Physiol* **272**, C1345-1351, doi:10.1152/ajpcell.1997.272.4.C1345 (1997).
61 Korohoda, W., Pietrzkowski, Z. & Reiss, K. Chloramphenicol, an inhibitor of mitochondrial protein synthesis, inhibits myoblast fusion and myotube differentiation. *Folia Histochem Cytobiol* **31**, 9-13 (1993).
62 Arany, Z. *et al.* The transcriptional coactivator PGC-1beta drives the formation of oxidative type IIX fibers in skeletal muscle. *Cell Metab* **5**, 35-46, doi:10.1016/j.cmet.2006.12.003 (2007).
63 Leone, T. C. *et al.* PGC-1alpha deficiency causes multi-system energy metabolic derangements: muscle dysfunction, abnormal weight control and hepatic steatosis. *PLoS Biol* **3**, e101, doi:10.1371/journal.pbio.0030101 (2005).
64 Lelliott, C. J. *et al.* Ablation of PGC-1beta results in defective mitochondrial activity, thermogenesis, hepatic function, and cardiac performance. *PLoS Biol* **4**, e369, doi:10.1371/journal.pbio.0040369 (2006).
65 Cai, X. *et al.* Alpha-ketoglutarate promotes skeletal muscle hypertrophy and protein synthesis through Akt/mTOR signaling pathways. *Sci Rep* **6**, 26802, doi:10.1038/srep26802 (2016).
66 Blomqvist, B. I., Hammarqvist, F., von der Decken, A. & Wernerman, J. Glutamine and alpha-ketoglutarate prevent the decrease in muscle free glutamine concentration and influence protein synthesis after total hip replacement. *Metabolism* **44**, 1215-1222 (1995).
67 Tazi, E. & Errihani, H. Treatment of cachexia in oncology. *Indian J Palliat Care* **16**, 129-137, doi:10.4103/0973-1075.73644 (2010).
68 Le-Rademacher, J. G., Crawford, J., Evans, W. J. & Jatoi, A. Overcoming obstacles in the design of cancer anorexia/weight loss trials. *Crit Rev Oncol Hematol* **117**, 30-37, doi:10.1016/j.critrevonc.2017.06.008 (2017).
69 Doles, J. D. *et al.* Does the Poly (ADP-Ribose) Polymerase Inhibitor Veliparib Merit Further Study for Cancer-Associated Weight Loss? Observations and Conclusions from 60 Prospectively Treated Patients. *J Palliat Med*, doi:10.1089/jpm.2018.0023 (2018).
70 von Haehling, S., Morley, J. E., Coats, A. J. S. & Anker, S. D. Ethical guidelines for publishing in the journal of cachexia, sarcopenia and muscle: update 2017. *J Cachexia Sarcopenia Muscle* **8**, 1081-1083, doi:10.1002/jcsm.12261 (2017).

742 **FIGURE LEGENDS**

743 **Figure 1: Modeling succinate accumulation and evaluating consequences**
744 **on growth and atrophy (A)** A bar graph depicting relative intracellular levels of
745 TCA metabolites in C2C12 myoblasts following 48h DM-succinate treatment as
746 determined by gas chromatography mass spectrometry (GC/MS) analyses.
747 *p<0.05. n=3 replicates. **(B)** Proliferation curve (measured as percent
748 confluence) for control, 4, 8, and 16 mM DM-succinate over 48 hours. Percent
749 confluence was averaged from 3 images per replicate, N= 6 replicate wells for
750 each condition. Error bars represent SEM. **(C)** Percent apoptotic cells, measured
751 by number of Annexin V positive cells, for control, 4, 8, and 16 mM DM-succinate
752 over 48 hours. Percent apoptotic cells was averaged from 3 images per replicate,
753 N=3 replicate wells for each condition. Error bars represent SD. **(D)** Bar graphs
754 quantifying Murf1 (left) and Atrogin1 (right) mRNA expression FC relative to D0-
755 growth media at 0, 1, 2, 3, and 4d in differentiation media +/- 8 mM DM-
756 succinate. *p<0.05 between control and succinate samples for marked
757 timepoints, as determined by multiple t tests with Holm-Sidak multiple testing
758 correction. **(E)** A bar graph showing reduced OPP accumulation in C2C12 cells
759 treated for 48h with 8mM DM-succinate. n=3 replicates; *p<0.05. **(F)** A graph of
760 myotube diameter measurements (microns) from C2C12 myotubes treated with
761 DM-succinate for 24h. n.s.=not significant (p>0.05) between any conditions
762 tested.

763 **Figure 2: Elevated succinate levels impair *in vitro* myogenesis (A)** RNA
764 sequencing analysis of proliferating C2C12 myoblasts treated with 8 mM DM-
765 succinate for 48 hours. Heatmap depicting normalized FPKM values for
766 myogenic and muscle lineage marker expression values. Blue=lower relative
767 expression, orange=higher relative expression. n=3 replicates for each condition.
768 **(B)** qPCR analysis of myogenic markers Pax7, MyoD1, Myog, and MyH1. Bar
769 graphs depicting mRNA expression FC relative to D0-growth media at 0, 1, 2, 3,
770 and 4d in differentiation media +/- 8 mM DM-succinate. n=3 replicates for each
771 timepoint/condition, *p<0.05 between control and succinate samples for marked
772 timepoints, as determined by multiple t tests with Holm-Sidak multiple testing

773 correction. **(C)** Representative images of C2C12 cultures in the presence of
774 differentiation media supplemented with 8mM DM-succinate for the entirety of
775 differentiation (5 days). Red depicts myosin heavy chain positive myocytes and
776 maturing myotubes. Nuclei are shown in blue (DAPI). Scale bar=100um. **(D)** A
777 graph depicting the number of nuclei per myosin heavy chain positive structure
778 (one point=one structure). Red=statistically significant ($p<0.05$) mean of
779 biological replicates compared to control using unpaired, nonparametric, Mann-
780 Whitney tests. n=4 replicates control/8mM DM-succinate, n=5 replicates 4mM
781 DM-succinate, 20-40 myotubes/replicate.

782 **Figure 3: Succinate supplementation impairs skeletal muscle homeostasis**
783 **(A)** Bi-weekly body weight tracking over 6-week succinate supplementation.
784 Weights are normalized to pre-supplementation baseline measures. Individual
785 points are individual animals, line represents the mean at each time point. **(B)**
786 Mouse weight at endpoint, normalized to pre-supplementation baseline
787 measures. **(C)** Bi-weekly echoMRI-measured lean mass normalized to pre-
788 supplementation baseline measures. Individual points are individual animals, box
789 represents the quartiles and whiskers represent the minimum and maximum
790 values. **(D)** Weights of tibialis anterior (TA) and gastrocnemius (GR) at endpoint
791 in milligrams. Individual points are individual animals, box represents the
792 quartiles and whiskers represent the minimum and maximum values. **(E)**
793 Representative images of TA muscle tissue sections from vehicle or succinate
794 supplemented mice after 6 weeks administration. Cross sections are
795 immunofluorescent stained with an antibody targeting laminin (white). Nuclei are
796 labeled with DAPI (blue). Scale bars=100 μm **(F)** Quantification of minimum feret
797 diameter of myofibers from vehicle and succinate supplemented mice. Feret
798 diameters were binned to a histogram and fit with a non-linear regression
799 (gaussian, least squares regression). Succinate exposed myofibers were
800 significantly smaller; $P< 0.0001$ by extra sun-of-squares F test. n.s. = not
801 significant by student's t test, n=7 vehicle, n=8 succinate-supplemented FVB
802 male mice, 4-5 months old at the start of the study.

803 **Figure 4: Succinate supplementation impairs skeletal muscle regeneration**

804 **(A)** Representative images of TA muscle tissue sections from vehicle or
805 succinate supplemented mice 7 days post 1.2% $BaCl_2$ injury stained with an
806 antibody targeting laminin (white). Nuclei are labeled with DAPI (blue). **(B)** A
807 histogram of myofiber feret diameters at 7 days post injury (dpi). Non-linear
808 regression and statistical analyses were performed as in Fig. 3, succinate injured
809 myofibers were ~16% smaller; p=0.0016. **(C)** Representative images of TA
810 muscle tissue sections from vehicle or succinate supplemented mice 28 days
811 post 1.2% $BaCl_2$ injury stained with an antibody targeting laminin (white). Nuclei
812 are labeled with DAPI (blue). **(D)** A histogram of myofiber feret diameters at 28
813 days post injury (dpi). Non-linear regression and statistical analyses were
814 performed as in Fig. 3, succinate injured myofibers were ~52% smaller;
815 p<0.0001. **(E)** Representative images of TA muscle tissue sections from vehicle
816 or succinate supplemented mice 28 dpi stained with antibodies targeting Pax7
817 (green), and Ki67 (red, upper panels), or Myogenin (red, lower panels). Nuclei
818 are labeled with DAPI (blue). Yellow arrows in upper panels point to Pax7+/Ki67+
819 cells. Yellow arrow heads in lower panels point to Myog+ cells. **(F)** Quantification
820 of Pax7+, Pax7+/Ki67+, and Myog+ cells per mm^2. Data represent the
821 quantification of a 0.844 mm^2 area per animal. Data points represent individual
822 animals. Box represents the inner quartiles and whiskers represent minimum and
823 maximum values. p values are represented in the figure, as determined by
824 unpaired student's t test. Mice were 3-4 months old, FVB males. n=5 mice 28dpi
825 vehicle; n=4 mice 28dpi succinate; n=5 mice 7dpi vehicle; n=3 mice 7dpi
826 succinate. Scale bars in panel 4A and 4C=100 um, 4E=50 μm.

827 **Figure 5: Succinate elevation impairs mitochondria function in myoblast**
828 **cells (A)** A bar chart depicting pathway enrichment analyses (sorted by p-value)
829 using HMDB IDs. Shown are the top 25 enriched processes. All data are derived
830 from Metaboanalyst processing of non-targeted analysis of C2C12 cells treated
831 with control or 8 mM DM-succinate media for 48 hours. n=3 control and n=3 8
832 mM DM-succinate. **(B)** A circular pie chart depicting the relative distribution of
833 differentially regulated metabolic pathways using HMDB IDs during function
834 explorer analysis. **(C)** Line graphs showing oxygen consumption rates (OCR),

835 normalized to cell count, of C2C12 myoblasts treated sequentially with
836 oligomycin (dashed line 1), FCCP (dashed line 2), and Antimycin A/Rotenone
837 (dashed line 3) in the presence or absence of 4 mM or 8 mM DM-succinate. **(D-**
838 **G)** Bar graphs displaying basal respiration rates (F), maximal respiration (G),
839 reserve capacity (H), and non-mitochondrial respiration (I). n=3; *$p<0.05$,
840 **$p<0.01$ by unpaired student's t-test**. (H)** Line graphs depicting OCR and ECAR
841 (extracellular acidification rate) in response to mitochondria stress (Energy
842 phenotype assay; Seahorse) in C2C12 control or DM-succinate treated
843 myoblasts. Filled circles are basal conditions, open circles are stressed
844 conditions. n=3 control and n=3 8 mM succinate.

Figure 1

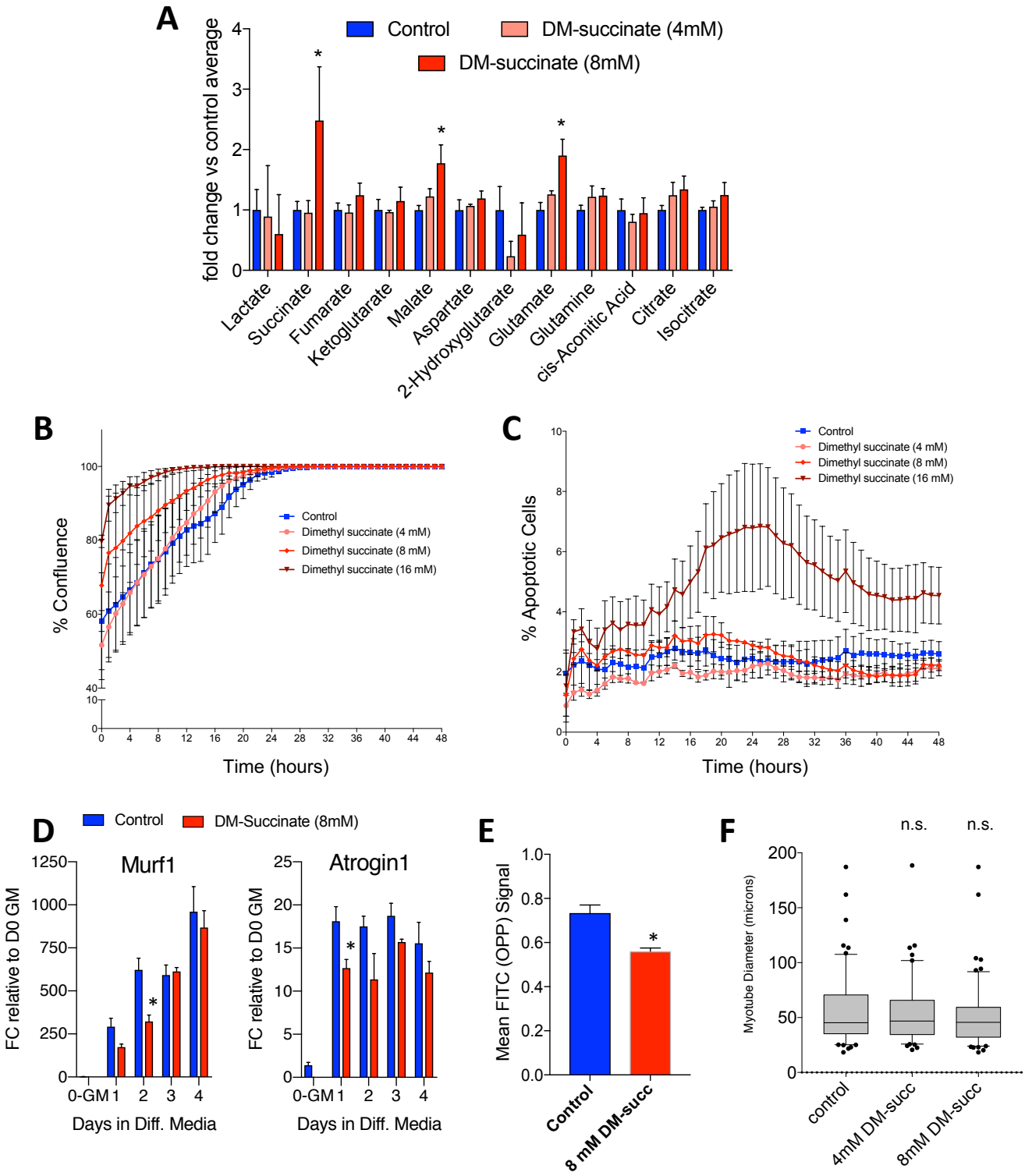
A
Control
DM-succinate (4mM)
DM-succinate (8mM)
fold change vs control average
Lactate
Succinate
Fumarate
Ketoglutarate
Malate
Aspartate
2-Hydroxyglutarate
Glutamate
Glutamine
cis-Aconitic Acid
Citrate
Isocitrate
B
% Confluence
Time (hours)
Control
Dimethyl succinate (4 mM)
Dimethyl succinate (8 mM)
Dimethyl succinate (16 mM)
C
% Apoptotic Cells
Time (hours)
Control
Dimethyl succinate (4 mM)
Dimethyl succinate (8 mM)
Dimethyl succinate (16 mM)
D
Control
DM-Succinate (8mM)
Murf1
Atrogin1
FC relative to D0 GM
Days in Diff. Media
E
Mean FITC (OPP) Signal
Control
8 mM DM-succ
F
n.s.
n.s.
Myotube Diameter (microns)
control
4mM DM-succ
8mM DM-succ

Figure 2

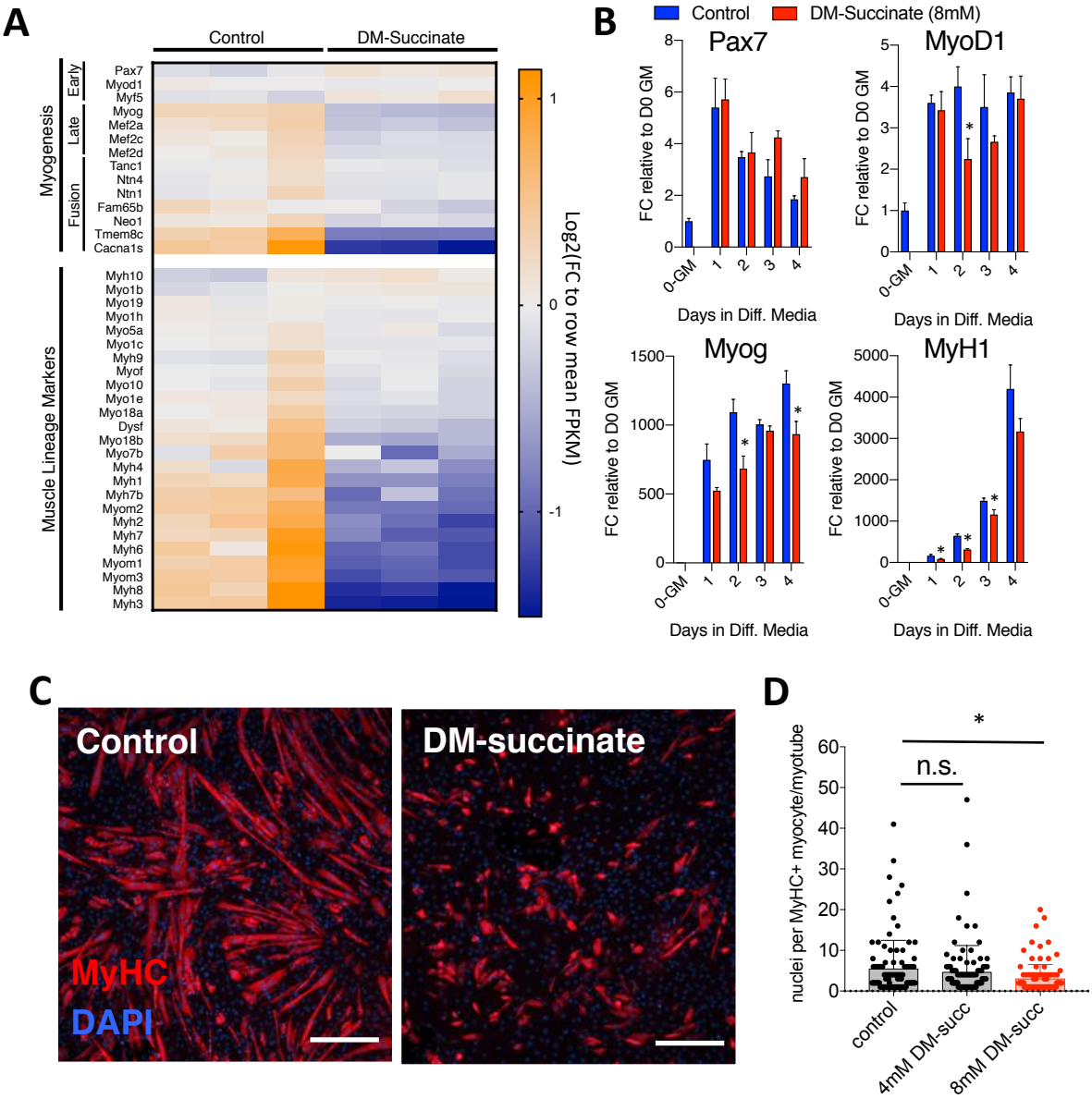
A
Control
DM-Succinate
Myogenesis
Early
Late
Fusion
Muscle Lineage Markers
Pax7
Myod1
Myf5
Myog
Mef2a
Mef2c
Mef2d
Tanc1
Ntn4
Ntn1
Fam65b
Neo1
Tmem8c
Cacna1s
Myh10
Myo1b
Myo19
Myo1h
Myo5a
Myo1c
Myh9
Myof
Myo10
Myo1e
Myo18a
Dysf
Myo18b
Myo7b
Myh4
Myh1
Myh7b
Myom2
Myh2
Myh7
Myh6
Myom1
Myom3
Myh8
Myh3
Log2(FC to row mean FPKM)
1
0
-1
B
Control
DM-Succinate (8mM)
Pax7
MyoD1
Myog
MyH1
FC relative to D0 GM
Days in Diff. Media
0-GM
1
2
3
4
C
Control
DM-succinate
MyHC
DAPI
D
nuclei per MyHC+ myocyte/myotube
n.s.
*
control
4mM DM-succ
8mM DM-succ

Figure 3

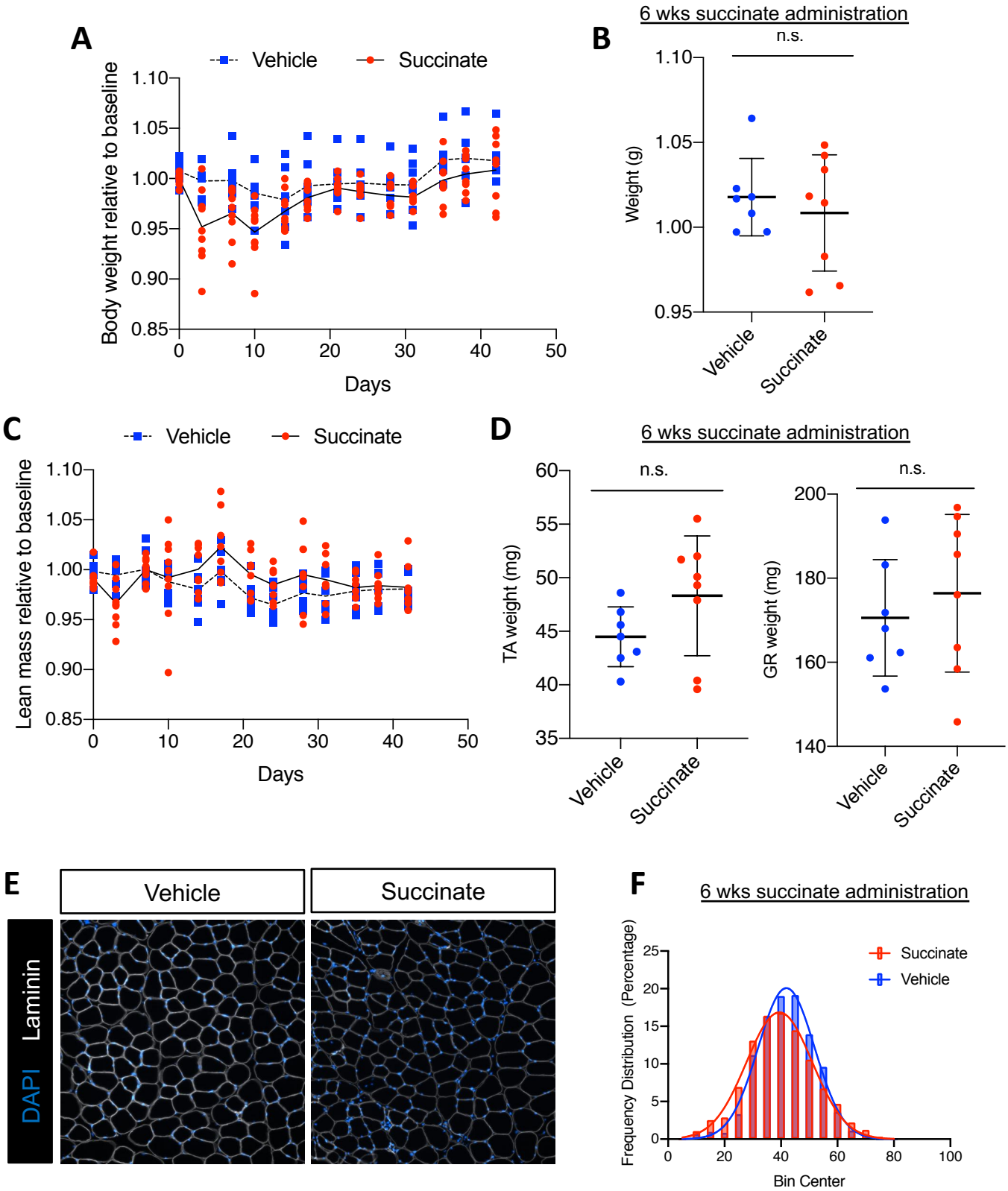
A
Vehicle
Succinate
Body weight relative to baseline
1.10
1.05
1.00
0.95
0.90
0.85
0
10
20
30
40
50
Days
B
6 wks succinate administration
n.s.
Weight (g)
1.10
1.05
1.00
0.95
Vehicle
Succinate
C
Vehicle
Succinate
Lean mass relative to baseline
1.10
1.05
1.00
0.95
0.90
0.85
0
10
20
30
40
50
Days
D
6 wks succinate administration
n.s.
TA weight (mg)
60
55
50
45
40
35
Vehicle
Succinate
n.s.
GR weight (mg)
200
180
160
140
Vehicle
Succinate
E
Vehicle
Succinate
Laminin
DAPI
F
6 wks succinate administration
Succinate
Vehicle
Frequency Distribution (Percentage)
25
20
15
10
5
0
0
20
40
60
80
100
Bin Center

Figure 4

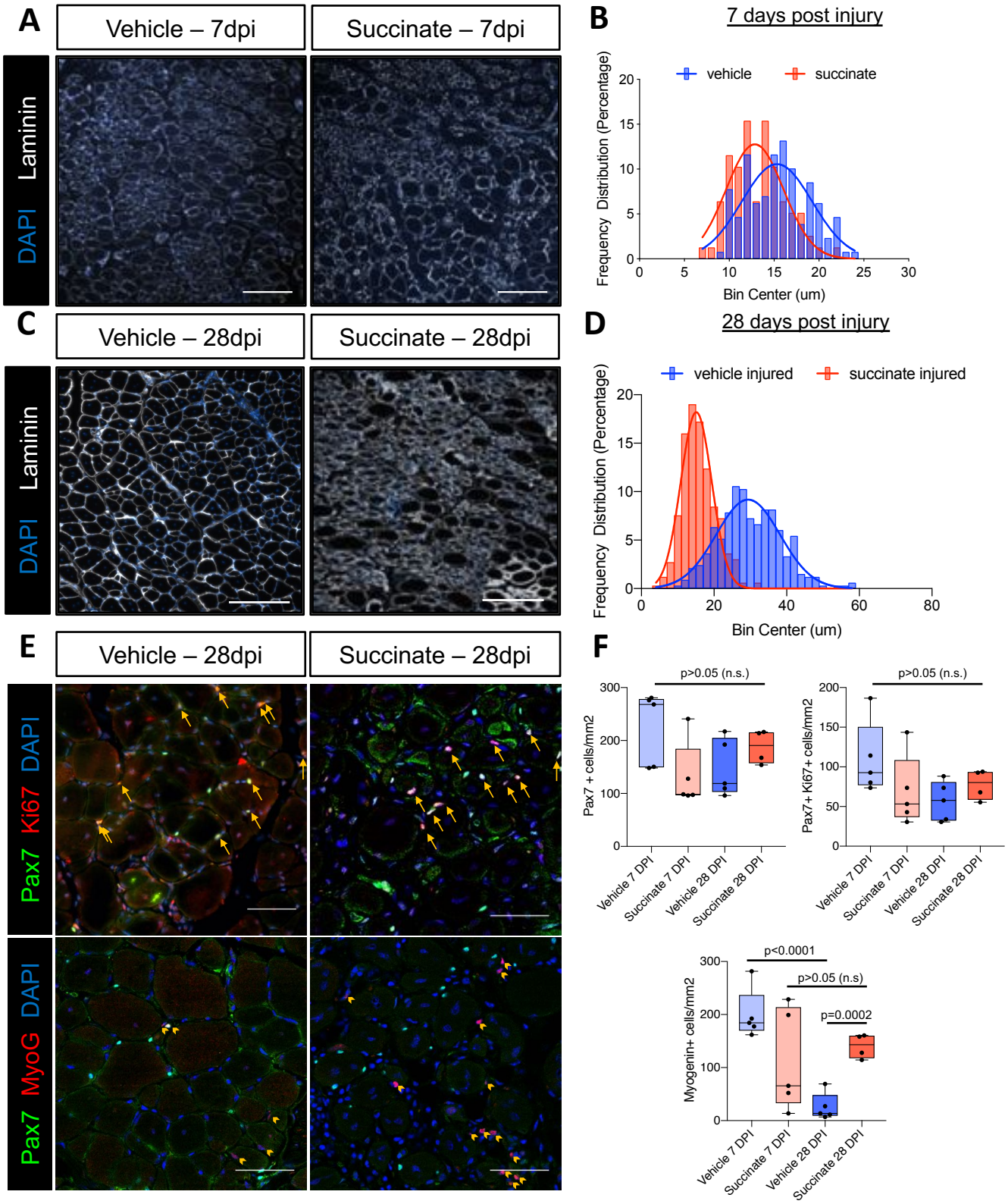
A
Vehicle – 7dpi
Succinate – 7dpi
Laminin
DAPI
B
7 days post injury
vehicle
succinate
Frequency Distribution (Percentage)
Bin Center (um)
C
Vehicle – 28dpi
Succinate – 28dpi
Laminin
DAPI
D
28 days post injury
vehicle injured
succinate injured
Frequency Distribution (Percentage)
Bin Center (um)
E
Vehicle – 28dpi
Succinate – 28dpi
Pax7 Ki67 DAPI
Pax7 MyoG DAPI
F
p>0.05 (n.s.)
Pax7 + cells/mm2
Pax7+ Ki67+ cells/mm2
Vehicle 7 DPI
Succinate 7 DPI
Vehicle 28 DPI
Succinate 28 DPI
p<0.0001
p>0.05 (n.s)
p=0.0002
Myogenin+ cells/mm2

Figure 5

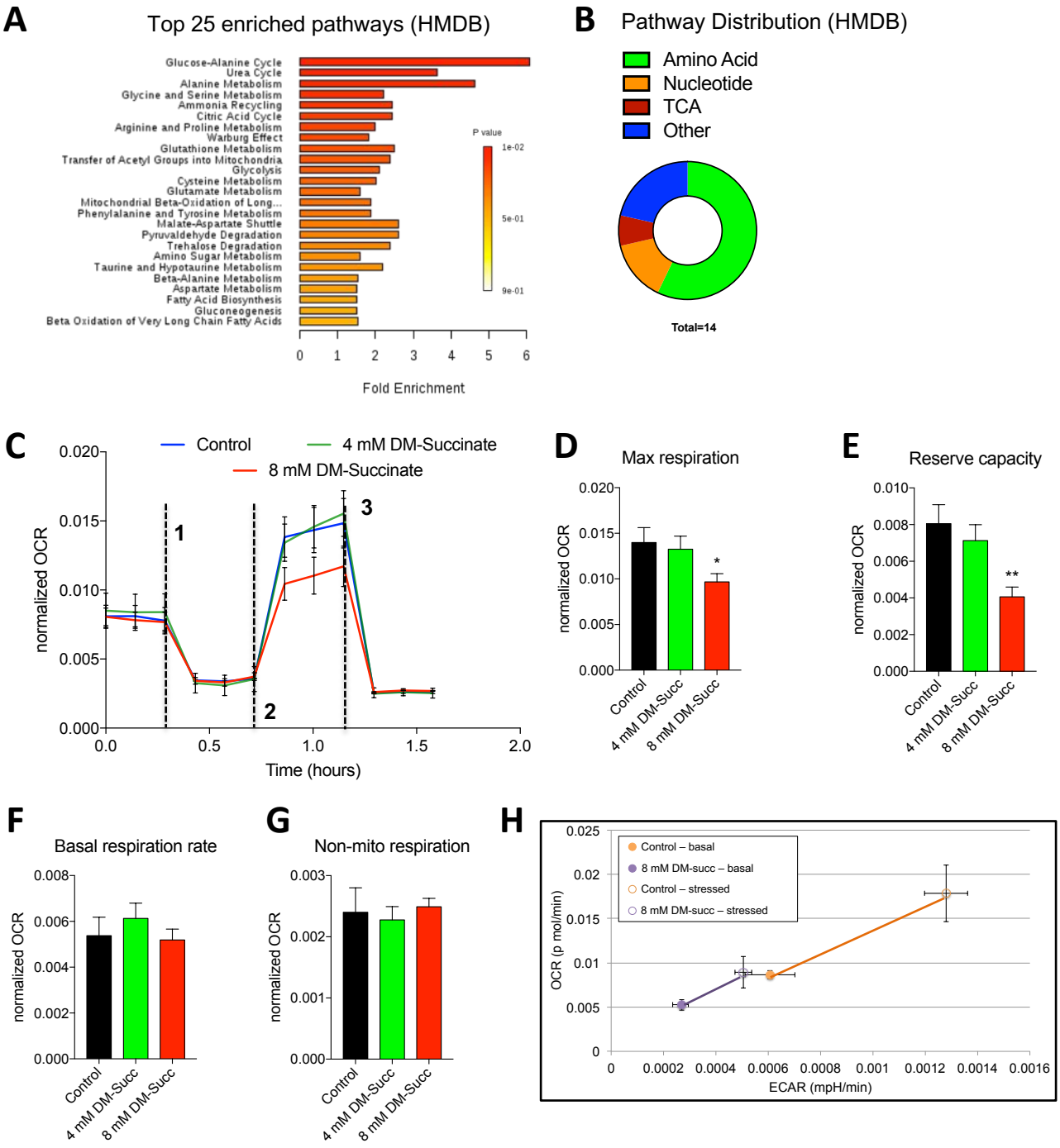
A
Top 25 enriched pathways (HMDB)
Glucose-Alanine Cycle
Urea Cycle
Alanine Metabolism
Glycine and Serine Metabolism
Ammonia Recycling
Citric Acid Cycle
Arginine and Proline Metabolism
Warburg Effect
Glutathione Metabolism
Transfer of Acetyl Groups into Mitochondria
Glycolysis
Cysteine Metabolism
Glutamate Metabolism
Mitochondrial Beta-Oxidation of Long...
Phenylalanine and Tyrosine Metabolism
Malate-Aspartate Shuttle
Pyruvaldehyde Degradation
Trehalose Degradation
Amino Sugar Metabolism
Taurine and Hypotaurine Metabolism
Beta-Alanine Metabolism
Aspartate Metabolism
Fatty Acid Biosynthesis
Gluconeogenesis
Beta Oxidation of Very Long Chain Fatty Acids
P value
1e-02
5e-01
9e-01
0 1 2 3 4 5 6
Fold Enrichment
B
Pathway Distribution (HMDB)
Amino Acid
Nucleotide
TCA
Other
Total=14
C
Control
4 mM DM-Succinate
8 mM DM-Succinate
normalized OCR
0.020
0.015
0.010
0.005
0.000
1
2
3
0.0 0.5 1.0 1.5 2.0
Time (hours)
D
Max respiration
normalized OCR
0.020
0.015
0.010
0.005
0.000
*
Control
4 mM DM-Succ
8 mM DM-Succ
E
Reserve capacity
normalized OCR
0.010
0.008
0.006
0.004
0.002
0.000
**
Control
4 mM DM-Succ
8 mM DM-Succ
F
Basal respiration rate
normalized OCR
0.008
0.006
0.004
0.002
0.000
Control
4 mM DM-Succ
8 mM DM-Succ
G
Non-mito respiration
normalized OCR
0.003
0.002
0.001
0.000
Control
4 mM DM-Succ
8 mM DM-Succ
H
Control – basal
8 mM DM-succ – basal
Control – stressed
8 mM DM-succ – stressed
OCR (p mol/min)
0.025
0.02
0.015
0.01
0.005
0
0 0.0002 0.0004 0.0006 0.0008 0.001 0.0012 0.0014 0.0016
ECAR (mpH/min)